2023 62nd IEEE Conference on Decision and Control (CDC)
December 13-15, 2023. Marina Bay Sands, Singapore

# A Trajectory Based Optimization Approach for Hybrid Observer design

F. Oliva, S. Mattogno, A. Tenaglia, R. Masocco, F. Martinelli, D. Carnevale

*Abstract*— **This paper presents a study on developing a hybrid 3D position observer for a rover with acceleration and relative distance measurements. The observer design utilizes two different methodologies; a Trajectory Based Optimization Design (TBOD) and a Linear Matrix Inequality (LMI) method. We prove that, under the proposed solutions, the boundedness of the estimation error is guaranteed. The performance of the observer is evaluated and compared to a standard EKF using comprehensive Monte Carlo simulations.**
*Index Terms*— **Hybrid systems; Optimization; Estimation**

## I. Introduction

The rise of interest in autonomous systems has put the spotlight on navigation, namely the capability of a robot to get an awareness of the surroundings and consequently decide on a motion control strategy to reach specific target locations successfully. Indeed, navigation strongly relies on localization algorithms, which estimate the agent's position and attitude. Depending on the goodness of the initial estimation, localization can be addressed as a position tracking or global localization problem [1]. Furthermore, localization is affected by the environment in which the robot moves; a dynamic environment substantially complicates the task. In this scenario, simultaneous localization and mapping (SLAM) algorithms are considered the standard [2].

Several technologies are used to address localization; position tracking and global localization exploit both internal sensors (e.g., IMU, gyros, encoders) and external sensors (e.g., GNSS, range sensors) [3]. A special mention should be made of the vision-based SLAM algorithms (V-SLAM), which use cameras [4]. The combined usage of different sensors is commonly referred to as sensor fusion [5], [6]; the solutions proposed in the literature vary from different fields, from observer theory to deep learning, handling nonlinear and multi-rate sensors. An interesting approach is the Markov localization, a probabilistic approach based on a discrete state-space representation [7].

Another solution widely used is the *Ultra Wide Band* (UWB) technology. These antennas can measure the relative distance between the object in question and the preset landmarks. In particular, the antenna mounted on the agent is called *tag*, while those identifying the landmarks are called *anchors*. The idea is to define points in the operating space that identify the reference system of the robot. At this point, the problem is to find the agent's position, knowing his distance from the different points. The problem has been approached in several ways: trilateration approaches (e.g., [8]) provide an initial estimation of the landmark position using three or more available range measurements. Other methods consider probabilistic grids as an accumulator voting scheme [9]. UWB localization and SLAM have been widely compared in [10], and visual-UWB navigation in unknown environments has been addressed in [11].

However, among probabilistic approaches, the Kalman filter (KF) represents the standard for sensor fusion and localization problems, along with all its improvements and modifications. In particular, the Extended Kalman Filter (EKF) is widely used to deal with sensor and model nonlinearity. In [12], low-cost GNSS and IMU sensors are exploited for precise 2D positioning. [13] uses distance measurements provided by Radars and Lidars instead. Regarding the multi-rate nature of a general sensor setup, KF-based algorithms can easily address it, as shown in [14]–[16]. Regarding the stability claims for EKF, key results have been proposed in [17]. The main drawback of KF-based approaches is the local linearization and the consistent computational burden.

In this scenario, Hybrid systems [18] can be considered a valid alternative to KF-based localization systems. More specifically, Hybrid observers have been proposed to deal with intermittent measurements in [19] and [20], [21]. In particular, [19] proposes a procedure for designing a static-gain hybrid observer on linear systems with known input and asynchronous measurements.

This paper deals with designing a hybrid 3D position observer for a rover with acceleration and relative distance measurements provided by IMU and UWB antennas, respectively. The main contributions of this work are the following:

- A linear hybrid observer is designed through an LMI-based procedure inspired by [19], based on knowledge of the plant control input, where two different dynamics are used between the plant and the observer. Moreover, the plant control input is unknown.
- A linear hybrid observer is designed through a Trajectory Based Optimization Approach (TBOD).

## II. Problem Statement

This section introduces the plant considered for the localization problem, the measurement setup, and the structure of the proposed observer. As presented in Section I, this work addresses the localization of a material point moving in a 3D environment. We are interested in designing a very fast

F. Oliva, S. Mattogno, A. Tenaglia, R. Masocco, F. Martinelli, D. Carnevale are with the Department of Civil Engineering and Computer Science Engineering, University of Rome "Tor Vergata", 00133 Rome, Italy. E-mails: {federico.oliva, simone.mattogno, alessandro.tenaglia, roberto.masocco, francesco.martinelli, daniele.carnevale}@uniroma2.it.

This work has been partially supported by the Italian Ministry for Research in the framework of the 2020 Program for Research Projects of National Interest (PRIN). Grant No. 2020RTWES4.

and lightweight observer capable of matching the estimation precision of the object's position from methods known in the literature and occasionally doing better. In particular, our goal is to maintain good precision on the $x, y$ axes while improving the estimation on the $z$ axis. The agent is represented as the following dynamic model $\mathcal{P}$, where the orientation dynamics are not considered for simplicity:

$$\mathcal{P} \; : \; \begin{cases} \dot{\boldsymbol{p}} &= \boldsymbol{v} \\ \dot{\boldsymbol{v}} &= \boldsymbol{u} \\ \dot{\boldsymbol{b}} &= 0, \end{cases} \rightarrow \dot{\boldsymbol{x}} = A\boldsymbol{x} + B\boldsymbol{u}, \tag{1a}$$

$$\boldsymbol{y} = \begin{bmatrix} \boldsymbol{d} \\ \boldsymbol{a} \end{bmatrix} = \begin{bmatrix} \boldsymbol{d}^\star \\ \boldsymbol{u} \end{bmatrix} + \begin{bmatrix} \boldsymbol{\nu}_d \\ \boldsymbol{b} + \boldsymbol{\nu}_a \end{bmatrix}, \tag{1b}$$

where $\boldsymbol{x} = [\boldsymbol{p}^T \; \boldsymbol{v}^T \; \boldsymbol{b}^T]^T \in \mathbb{R}^9$ is the plant state vector, $\boldsymbol{p}, \boldsymbol{v} \in \mathbb{R}^3$ are the position and velocity of the rover, respectively, $\boldsymbol{u} \in \mathbb{R}^3$ is the unknown input of the plant, and $\boldsymbol{b} \in \mathbb{R}^3$ is a measurement bias that will be detailed later. $\boldsymbol{y} \in \mathbb{R}^{N+3}$ is the vector of plant outputs: measurements consisting of the signal provided by an IMU $\boldsymbol{a} \in \mathbb{R}^3$, and a set of range measurements $\boldsymbol{d} = [d_1, \dots, d_N]^T \in \mathbb{R}^N$ provided by $N$ fixed UWB antennas placed at known locations, called *anchors*, and one antenna installed on the agent, called *tag*. Lastly, $\boldsymbol{\nu}_d \in \mathbb{R}^N$ and $\boldsymbol{\nu}_a \in \mathbb{R}^3$ are the measurement noises. The ranging measurements are defined as $d_i^\star = \|\boldsymbol{p}_{A,i} - \boldsymbol{p}\|$, where $\boldsymbol{p}_{A,i} \in \mathbb{R}^3$ is the known absolute position of the $i$-th anchor and $\boldsymbol{p}$ is the position of the tag installed on the object[1]. Regarding the ranging measurements, we also let *Assumption 2* from [22] to hold, i.e., at least three non-collinear anchors are available at any time. Regarding the IMU measurements $\boldsymbol{a}$, we assume that $\boldsymbol{a} = \boldsymbol{u} + \boldsymbol{b} + \boldsymbol{\nu}_a$, as in (1b), where $\boldsymbol{b}$ denotes the measurement bias previously introduced.

As we are tackling an estimation problem for real applications, we assume that the output $\boldsymbol{y}$ is sampled by multi-rate acquisition hardware. Indeed, IMU and UWB measurements are available with different rates, $\Delta t_a$ and $\Delta t_d$, respectively defined as

$$t_{\boldsymbol{a},q} - t_{\boldsymbol{a},q-1} = \Delta t_a, \tag{2a}$$

$$t_{\boldsymbol{d},l} - t_{\boldsymbol{d},l-1} = \Delta t_d, \tag{2b}$$

where $(q, l) \in \mathbb{N}$, $\Delta t_a \leq \Delta t_d$ and $\Delta t_d = h\Delta t_a$, with $h \in \mathbb{N}_0 \gg 1$. Under this assumption, we consider the IMU acquisition to be continuous compared to the UWB. Thus, the hybrid framework is used, considering the IMU dynamics continuous and the UWB correction discrete.

To propose a hybrid observer, analogously to [19], we model the plant $\mathcal{P}$ as a hybrid system $\mathcal{P}_h$, exploiting the formalism proposed in [18], with continuous and discrete time dynamics

$$\mathcal{P}_h : \begin{cases} \dot{\boldsymbol{x}} &= A\boldsymbol{x} + B\boldsymbol{u} \\ \dot{\tau} &= 1 \end{cases}, \quad (\boldsymbol{x}, \tau) \in \mathcal{C}, \tag{3a}$$

$$\begin{cases} \boldsymbol{x}^+ &= \boldsymbol{x} \\ \tau^+ &= 0 \end{cases}, \quad (\boldsymbol{x}, \tau) \in \mathcal{D},$$

[1]We assume that the tag position is the position of the object.

where $\mathcal{C} \triangleq \{x \in \mathbb{R}^9, \tau \in [0, \Delta t_d)\}$ and $\mathcal{D} \triangleq \{x \in \mathbb{R}^9, \tau \geq \Delta t_d\}$. The continuous-time evolution of the system is described by a flow-map defined over the set $\mathcal{C}$. The discrete-time evolution is instead described by a jump-map defined over the set $\mathcal{D}$. The timer variable $\tau \in \mathbb{R}$ keeps track of the flow time between each state reset, namely, each switch between these maps. Here, note that the jump-map is not used to change the dynamics, as a continuous-time system describes the plant. Instead, the hybrid framework will come in handy when describing the observer structure, which will rely on continuous and discrete-time IMU and UWB acquisitions, respectively.

As introduced in Section I, our objective is to design a hybrid observer for $\mathcal{P}_h$, where the input $\boldsymbol{u}$ is considered unknown. Then, consider the following continuous-time system:

$$\hat{\mathcal{P}} \; : \; \begin{cases} \dot{\hat{\boldsymbol{p}}} &= \hat{\boldsymbol{v}} \\ \dot{\hat{\boldsymbol{v}}} &= \hat{\boldsymbol{a}} - \hat{\boldsymbol{b}} \\ \dot{\hat{\boldsymbol{b}}} &= 0 \\ \dot{\hat{\boldsymbol{a}}} &= \alpha(\boldsymbol{a} - \hat{\boldsymbol{a}}) \end{cases} \rightarrow \dot{\hat{\boldsymbol{x}}} = A_h\hat{\boldsymbol{x}} + B_h\boldsymbol{a}, \tag{4}$$

where $\hat{\boldsymbol{x}} = [\hat{\boldsymbol{p}}^T \; \hat{\boldsymbol{v}}^T \; \hat{\boldsymbol{b}}^T \; \hat{\boldsymbol{a}}^T]^T \in \mathbb{R}^{12}$ is the observer state with $\hat{\boldsymbol{p}}, \hat{\boldsymbol{v}} \in \mathbb{R}^3$ respectively the estimated position and velocity, $\hat{\boldsymbol{b}}$ the estimated IMU bias, and $\hat{\boldsymbol{a}}$ the output of a low-pass filter of the IMU measurements $\boldsymbol{a}$. We define a signal $\boldsymbol{\nu}_f(t)$ in order to rewrite $\hat{\boldsymbol{a}}$ as

$$\hat{\boldsymbol{a}} = \boldsymbol{u} + \boldsymbol{b} + \boldsymbol{\nu}_f, \tag{5}$$

where $\boldsymbol{\nu}_f$ takes into account the mismatch between $\boldsymbol{a}$ and $\hat{\boldsymbol{a}}$ introduced by the linear dynamics of $\hat{\boldsymbol{a}}$ in (4) and the Gaussian noise measurement $\boldsymbol{\nu}_a$ in (1b). We now propose the hybrid observer $\hat{\mathcal{P}}_h$ for $\mathcal{P}_h$ with hybrid dynamics, defined as:

$$\hat{\mathcal{P}}_h : \begin{cases} \dot{\hat{\boldsymbol{x}}} &= A_h\hat{\boldsymbol{x}} + B_h\boldsymbol{a} \\ \dot{\tau} &= 1 \end{cases}, \quad (\hat{\boldsymbol{x}}, \tau) \in \hat{\mathcal{C}}, \tag{6}$$

$$\begin{cases} \hat{\boldsymbol{x}}^+ &= \hat{\boldsymbol{x}} + \tilde{\mathbf{K}}(g(\boldsymbol{d}) - \hat{\boldsymbol{p}}) \\ \tau^+ &= 0 \end{cases}, \quad (\hat{\boldsymbol{x}}, \tau) \in \hat{\mathcal{D}}$$

where $\hat{\mathcal{C}} \triangleq \{\hat{x} \in \mathbb{R}^{12}, \tau \in [0, \Delta t_d)\}$ and $\hat{\mathcal{D}} \triangleq \{\hat{x} \in \mathbb{R}^{12}, \tau \geq \Delta t_d\}$. Without loss of generality, within our framework, the timer variable $\tau$ is considered the same for all hybrid systems. Then, the dependence of the jump-map on the UWB measurements justifies the hybrid framework. Specifically, note that a static gain $\mathbf{K} \in \mathbb{R}^{9\times3}$ is introduced in the jump-map as an output injection term of the observer through $\tilde{\mathbf{K}} \in \mathbb{R}^{12\times3}$, $\tilde{\mathbf{K}} = \left[\mathbf{K}', 0_{3\times3}\right]'$. Differently from a standard EKF approach, $\hat{\mathcal{P}}_h$ does not require any model linearization or matrix inversion, which are both computed in the *prediction* and *correction* steps of the KF methods. Thus, the computational cost is lower in $\hat{\mathcal{P}}_h$.

The nonlinear map $g(\cdot) : \mathbb{R}^N \rightarrow \mathbb{R}^3$ represents the output of a trilateration algorithm that provides an estimate of the absolute position $\bar{\boldsymbol{p}}$ exploiting the ranging measurements $\boldsymbol{d}$ defined as

$$\bar{\boldsymbol{p}} = \arg\min_{\boldsymbol{p}} \sum_{i=1}^{N} (\|\boldsymbol{p}_{A,i} - \boldsymbol{p}\| - d_i)^2 = \arg\min_{\boldsymbol{p}} \mathrm{J}(\boldsymbol{p}). \quad (7)$$

Indeed, the solution to (7) can be computed either in closed form or numerically (see also [23]). An efficient algorithm to solve the trilateration problem, especially in the framework considered in this work, is the Newton-Raphson algorithm, which exhibits local quadratic convergence to (one of the) minimum of J, and whose single-step evaluation at the i-th iteration is defined as

$$\boldsymbol{p}_{i+1} = \boldsymbol{p}_i - \left(H_{\mathrm{J}}(\boldsymbol{p}_i)\right)^{-1} \nabla \mathrm{J}(\boldsymbol{p}_i), \quad (8)$$

where $H_{\mathrm{J}}$ is the Hessian matrix of J and $\nabla$J its gradient, both calculated with respect to $\boldsymbol{p}$. The Hessian shall be invertible over the trajectories considered. It can be easily shown through some calculations that the condition for this to happen consists of not having the material point to exactly reach the location of any fixed anchors, namely $\boldsymbol{p} = \boldsymbol{p}_A$, which never occurs in the trajectories considered in this work.

With the simulation settings of this work specified in V-A, iterating no more than five times the Newton-Raphson algorithm (8) yields a very accurate, although approximated, solution of (7), which we will refer to as $\boldsymbol{p}_5$. We then make the following assumption in the rest of the paper.

*Assumption 1:* Let $\boldsymbol{p} \in \Omega_p \subset \mathbb{R}^3$, with $\Omega_p$ and $\boldsymbol{\nu}_d$ bounded. Define $g(\boldsymbol{d}) \triangleq \boldsymbol{p}_5$, where $\boldsymbol{p}_5$ is obtained by five iterations of the Newton-Raphson algorithm (8), with initial condition $\boldsymbol{p}_0$, and assume that

$$\boldsymbol{p}_5 = \boldsymbol{p} + \boldsymbol{\nu}_J(\boldsymbol{\nu}_d), \quad (9)$$

holds true for any $\boldsymbol{p}_0 \in \Omega_p$, with a bounded function $\boldsymbol{\nu}_J : \mathbb{R}^N \to \mathbb{R}^3$ that takes into account the uncertainties introduced by the UWB ranging sensors, due to the measurement noise $\boldsymbol{\nu}_d$, and the approximate solution to (7) provided by five iterations of the Newton-Raphson algorithm.

We proceed now with the design of $\mathbf{K}$ such that the hybrid observer $\hat{\mathcal{P}}_h$ would provide estimates of $(\boldsymbol{p}, \boldsymbol{v}, \boldsymbol{b})$. Note that differently from [19], $\mathcal{P}_h$ and $\hat{\mathcal{P}}_h$ have different flow and jump maps. Moreover, the innovation term in (6) does not directly depend on the agent's position but rather on the ranging measurements. Indeed, the design of the static gain shall take these aspects into account. The following sections address the stability conditions for the proposed estimation problem and the design of a suitable static gain $\mathbf{K}$.

## III. Stability Analysis

In this Section, we analyze the estimation error dynamics. Let the estimation error be defined as:

$$\boldsymbol{e} = \begin{bmatrix} \boldsymbol{p} - \hat{\boldsymbol{p}} \\ \boldsymbol{v} - \hat{\boldsymbol{v}} \\ \boldsymbol{b} - \hat{\boldsymbol{b}} \end{bmatrix} \in \mathbb{R}^9. \quad (10)$$

Through some simple calculations and by Assumption 1, the error dynamics can be shown to be described by the hybrid system

$$\mathcal{E}_h : \begin{cases} \begin{cases} \dot{\boldsymbol{e}} &= A_e \boldsymbol{e} + B_e \boldsymbol{\nu}_f \\ \dot{\tau} &= 1 \end{cases}, & (\boldsymbol{e}, \tau) \in \mathcal{C}_e, \\ \begin{cases} \boldsymbol{e}^+ &= (\mathbf{I} - \boldsymbol{\Gamma}_K)\boldsymbol{e} - \mathbf{K}\boldsymbol{\nu}_J \\ \tau^+ &= 0 \end{cases}, & (\boldsymbol{e}, \tau) \in \mathcal{D}_e, \end{cases} \quad (11)$$

where:
$\mathcal{C}_e \triangleq \{\boldsymbol{e} \in \mathbb{R}^9, \tau \in [0, \Delta t_d)\}$, $\mathcal{D}_e \triangleq \{\boldsymbol{e} \in \mathbb{R}^9, \tau \geq \Delta t_d\}$, and

$$A_e = \begin{bmatrix} 0 & \mathbf{I}_3 & 0 \\ 0 & 0 & -\mathbf{I}_3 \\ 0 & 0 & 0 \end{bmatrix}, \quad B_e = \begin{bmatrix} 0 \\ -\mathbf{I}_3 \\ 0 \end{bmatrix}, \quad C_e = [\mathbf{I}_3 \ 0 \ 0],$$
$$\boldsymbol{\Gamma}_K = \mathbf{K} C_e = \begin{bmatrix} k_1\mathbf{I}_3 & \mathbf{0}_3 & \mathbf{0}_3 \\ k_2\mathbf{I}_3 & \mathbf{0}_3 & \mathbf{0}_3 \\ k_3\mathbf{I}_3 & \mathbf{0}_3 & \mathbf{0}_3 \end{bmatrix}, \quad \mathbf{K} = \begin{bmatrix} k_1\mathbf{I}_3 \\ k_2\mathbf{I}_3 \\ k_3\mathbf{I}_3 \end{bmatrix}, \quad (12)$$

and we wrap the scalar terms in a vector $K = [k_1 \ k_2 \ k_3]^T \in \mathbb{R}^3$. Thus, the design will consider $K$ only. Note that the output injection term entering in the jump map of the hybrid observer (3) together with Assumption 1 provides a correction term in the jump map of the estimation error system that depends on $\boldsymbol{d}$. The following theorem addresses the boundedness of the estimation error trajectories.

*Theorem 1:* Consider the hybrid system $\mathcal{P}_h$ and the observer $\hat{\mathcal{P}}_h$. Let Assumption 1 hold, and assume that there exists a positive constant $\overline{M} \in \mathbb{R}$ such that $\max\{\|u\|, \|\dot{u}\|, \boldsymbol{\nu}_a, \boldsymbol{\nu}_f, \boldsymbol{\nu}_d \ \boldsymbol{\nu}_J\} \leq \overline{M}$. Then, the origin of the estimation error system $\mathcal{E}_h$ is Globally Uniformly Ultimately Bounded.

*Remark 1:* Note that the bound on the error trajectories is related to the constant $\overline{M}$. The lower $\overline{M}$, the lower the bound. This suggests that better sensors can provide a smaller bound on the error trajectories, which is fair. Indeed, we intend to dig into this aspect in future developments.

Theorem 1 provides a set of constraints on the static-gain $K$. In the next section, we address the selection of $K$, such that the stability of $\mathcal{E}_h$ is ensured from Theorem 1.

## IV. Observer Design

This section presents two methods to obtain the static-gain $K$ introduced in Sections II and III. The first method follows [19], while the second relies on a trajectory mismatch optimization approach. The stability of $\mathcal{E}_h$ for the outcomes of both the methods is analyzed through the result of Theorem 1.

### A. LMI design method

The first method relies on the results presented in [19], and more specifically in *Proposition 1*, which we briefly recall:

*Proposition 1:* Consider system $\mathcal{E}_h$, a positive value $\Delta t_d > 0$, and a symmetric positive definite matrix $P = P^T > 0$. The problem described by [Eq. 13, [19]] is feasible if and only if the pair $(C_e, e^{A_e \Delta t_d})$ is detectable:

where $C_e$ is full row rank, and $C_e^{\perp}$ is a basis of the orthogonal complement of $C_e^T$.
Note that this work deals with synchronous measurements; $\Delta t_d$ is the only sampling time for the ranging sensors. Thus, [Eq. 13, [19]] is finite-dimensional. The solution $P$ to [Eq. 13, [19]] can be computed with the algorithm proposed in [19]. Then, the static gain $K$ is computed applying *Theorem 2* of [19].
As previously highlighted, differently from [19], here, the nominal and observer plants $\mathcal{P}$ and $\hat{\mathcal{P}}$ have different structures and dimensions. Moreover, the control input $\boldsymbol{u}$ is assumed to be unknown. Indeed, by rephrasing the estimation error definition as in (10), and considering $g(\boldsymbol{d})$ provided by Newton-Raphson as a position measure, we recast the localization problem to be compatible with the setup addressed in [19], which is the first contribution of this work.
We solved [Eq. 13, [19]] on $\mathcal{E}_h$ with the `gevp` `MATLAB` method, as suggested in [19]. The static gain $K^\star$ computed with [Eq. 17, [19]] resulted in $K^\star = [1, 1.2662, -0.5457]^T$, which can be easily checked to render $(\mathbf{I}-\mathbf{\Gamma}_{K^\star})e^{A_e \Delta t_d}$ Schur, and resulting in boundedness for $\mathcal{E}_h$ from Theorem 1. More specifically, it results $\left|\sigma((\mathbf{I}-\mathbf{\Gamma}_K)e^{A_e \Delta t_d})\right| = [0, 0.87, 0.87]^T$. One aspect stands out from this solution; $K^\star$ fully exploits the position measure $g(\boldsymbol{d})$ in the jump map, namely

$$\hat{x}_1^+ = \hat{x}_1 + k_1(g(\boldsymbol{d}) - \hat{x}_1) = g(\boldsymbol{d}). \tag{13}$$

This makes perfect sense if no measurement noise is considered, namely $\boldsymbol{\nu}_J = 0$. In such a case, the position error $\boldsymbol{p} - \hat{\boldsymbol{p}}$ vanishes after the first state-reset of $\hat{P}_h$. This is consistent with the zero eigenvalue. The performance of $K^\star$ both in absence and presence of noise is investigated in Section V.
Indeed, the LMI-based design method proposed in [19] does not consider any information on the measurement noise, as it relies on [Eq. 13, [19]]. Generally speaking, this approach could lead to poor estimation precision due to its lack of robustness. Thus, we propose another design approach to solve this issue.

### B. TBOD design method

This section describes the main methodological novelty of this work. The core idea is to formulate the static-gain design as an optimization problem. More specifically, consider $M$ different trajectories $(\boldsymbol{x}_j, \hat{\boldsymbol{x}}_j)$ for $(\mathcal{P}_h, \hat{\mathcal{P}}_h)$ within a time interval $[0\ T]$, and $j \in \{1, \dots, M\}$. The related estimation error trajectories are $\boldsymbol{e}_j = \boldsymbol{x}_j - \hat{\boldsymbol{x}}_j$. Indeed, from (11), $\boldsymbol{e}_j$ depends on the static-gain $K$ choice. Thus, we define the following optimization problem:

$$\overline{K} = \arg\min_K \quad \sum_{j=1}^{M} \int_0^T \|\boldsymbol{y}_{e,j}(t)\|\, dt \quad . \tag{14}$$

Indeed, differently from IV-A, the design takes into account measurement noise, as it relies on the actual error trajectories $\boldsymbol{e}_j$, directly affecting the output $\boldsymbol{y}_{e,j}$ of system $\mathcal{E}_h$ through $C_e$. Problem (14) has been defined over a set of trajectories $\boldsymbol{e}_j$ to further increase the robustness of the design by considering different initial conditions and evolutions for $\mathcal{E}_h$. Considering the structure of (14), this method is referred to as *Trajectory-Based Optimization Design* (TBOD).
Clearly, (14) defines a continuous-time problem as it considers the integral of $\boldsymbol{y}_{e,j}$. However, in the actual implementation, $\boldsymbol{y}_{e,j}$ is available at a specific rate: every $\Delta t_a$. Thus, (14) is implemented as

$$\overline{K} = \arg\min_K \quad \sum_{j=1}^{M} \sum_{p=1}^{P} \|\boldsymbol{y}_{e,j}(t_{\boldsymbol{a},p})\| \quad , \tag{15}$$

with $\Delta t_a$ chosen according to the Nyquist criterion, and $P = T/\Delta t_a$ the number of measurement samplings.
Indeed, the main drawback of the TBOD approach is the computational cost, which scales quickly with trajectories and system complexity. However, this issue affects only the offline computation time for $\overline{K}$. Before proceeding with the numerical results of this approach, some aspects should be highlighted.
*Remark 2:* The characteristics (e.g., convexity) of problem (15) strongly depend on the plant dynamics. Thus, its solution is generally agnostic to the minimization algorithm used. However, convergence speed can be increased under specific assumptions (e.g., linear dynamics and output mapping). Note that in this work, the Newthon-Rapshon method in (8) introduces a nonlinearity in $\hat{\mathcal{P}}_h$. Thus, we solved (15) with `MATLAB` built-in simplex-like `patternsearch` method.
*Remark 3:* As problem (15) is unconstrained, no general claims can be made on the stability of each trajectory $\boldsymbol{e}_j$. Thus, the stability of $\mathcal{E}_h$ with the obtained $\overline{K}$ is investigated a posteriori exploiting Theorem 1.
Note that, generally speaking, the TBOD method gives more design freedom compared to the LMI method, as it does not depend on the linearity of the plants $\mathcal{P}_h, \hat{\mathcal{P}}_h$. For instance, nonlinear update laws can be designed in place of static gain $K$.
The solution of problem (15) depends on the setup considered for plant $\mathcal{P}$. Thus, the detailed simulation setup and the obtained results are addressed in the dedicated Section V. Furthermore, the performance of LMI and TBOD methods are compared with a standard EKF filter.

## V. Results and Discussion

This section describes in detail the simulation setup for plant $\mathcal{P}$ and then proceeds by presenting the results of the TBOD design method. Lastly, a comparison of the LMI and TBOD performance is presented.

### A. Simulation setup

The simulation setup considers the position estimate of a terrestrial rover moving in an indoor 3D environment of dimensions roughly of $10 \times 15 \times 3$ m. Precisely, the area is filled with sparse hills around 50 cm high. The rover patrols the area by following a rectangular path. Four UWB antennas have been placed at a 2 m height and around the area.
Due to the patrolling task, the rover moves slowly, with velocities of around 0.5 m/s and with acceleration peaks of 0.5

m/s$^2$. Regarding the IMU and UWB sensors measurements, the sampling frequencies have been set respectively to 100 Hz for the IMU and 5 Hz for the UWB, resulting in $\Delta t_a = 0.01$ s, and $\Delta t_d = 0.2$ s, resulting in a factor $h = 20$ (see Section II). Noise characteristics have been defined as follows:

- IMU bias: for each trajectory $\boldsymbol{x}_j$, the IMU bias $\boldsymbol{b}_j$ is uniformly randomly selected within the interval $[0.05\ 0.15]$ m/s$^2$.
- IMU noise: the additive noise $\boldsymbol{\nu}_a$ is randomly selected from a zero-mean Gaussian distribution $\mathcal{N}(0, 0.05)$ m/s$^2$.
- UWB noise: the additive noise $\boldsymbol{\nu}_d$ is randomly selected from a zero-mean Gaussian distribution $\mathcal{N}(0, 0.2)$ m. The measurement precision has been selected accordingly to the UWB antennas DW1001 datasheet from *Qorvo* [2], where also bias correction was considered.

As for the direct rover position measurement $g(\boldsymbol{d})$, the additive noise $\boldsymbol{\nu}_J$ is of the same order of magnitude as $\boldsymbol{\nu}_d$.

### B. TBOD design

This paragraph describes the conditions used to define problem (15), and discusses its solution. More specifically, (15) has been defined over a set of $M = 5$ trajectories, each lasting $T = 200$ s, enough for the rover to cover the full area once. On each plant trajectory $\boldsymbol{x}_j$, the rover starts from a position $\boldsymbol{p}_{0,j}$ placed in the upper-right corner of the area, with zero velocity and acceleration. The initial condition $\hat{\boldsymbol{x}}_{0,j}$ of each estimated trajectory is set to $[\hat{\boldsymbol{p}}_{0,j}^T\ \hat{\boldsymbol{v}}_{0,j}^T\ \hat{\boldsymbol{b}}_{0,j}^T\ \hat{\boldsymbol{a}}_{0,j}^T]^T = [\boldsymbol{p}_{0,j}^T(1+\boldsymbol{\delta}_j)\ \mathbf{0}_{3\times1}^T\ \mathbf{0}_{3\times1}^T\ \mathbf{0}_{3\times1}^T]^T$, with each component of $\boldsymbol{\delta}_j \in \mathbb{R}^3$ extracted from a Gaussian distribution $\mathcal{N}(0, 0.5)$.
With these assumptions, problem (15) has been solved numerically with the built-in `MATLAB` method `patternsearch`, as introduced in Section IV.
The resulting static gain is $\overline{K} = [0.4221, 0.2888, -0.0281]^T$, which renders $(\mathbf{I} - \mathbf{\Gamma}_{\overline{K}})e^{A_e \Delta t_d}$ Schur, and more specifically $|\sigma((\mathbf{I} - \mathbf{\Gamma}_{\overline{K}})e^{A_e \Delta t_d})| = [0.7132, 0.8294, 0.9770]^T$.
In this case, there are no zero eigenvalues, meaning that the observer does not fully trust the measurements, providing more robustness to the estimation.

### C. LMI vs TBOD comparison

This paragraph compares the results of the static-gain obtained with the LMI and TBOD methods, namely $K^\star$ and $\overline{K}$. A first comparison is presented without measurement noise to show the convergence properties of the observer $\hat{\mathcal{P}}_h$. Then, the two gains are tested in the presence of measurement noise, and their performance is also compared to a standard EKF. The comparison has been made on a batch of 50 Monte Carlo simulations to validate the results.
*Noisy case:* The performance of the two gains with measurement noise is reported in Figure 1. Note that the saw-tooth behavior of the estimation error in Figure 1a is caused by the state reset. Indeed, every $\Delta t_d$, position, velocity, and bias are updated with the injection term $\mathbf{K}(g(\boldsymbol{d}) - \hat{\boldsymbol{p}})$. The free evolution in the subsequent time interval $[0, \Delta t_d]$ depends on the estimation of $\hat{\boldsymbol{a}}$, which eventually converges to $\boldsymbol{a}$ with

[2] https://www.qorvo.com/products/d/da007946

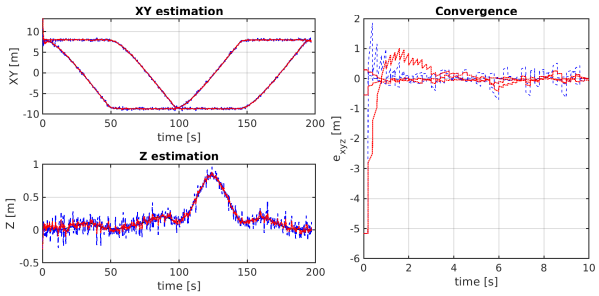


(a) $(\boldsymbol{p}, \hat{\boldsymbol{p}})$

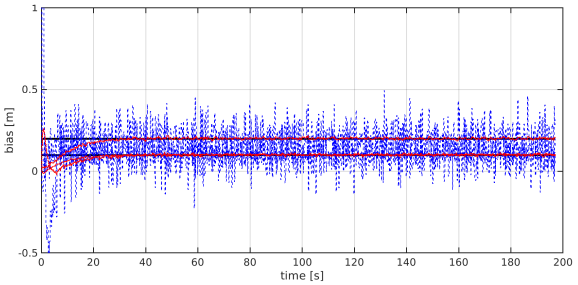


(b) $(\boldsymbol{b}, \hat{\boldsymbol{b}})$

Fig. 1: Estimation of $\boldsymbol{x}$ (solid black) with $K^\star$ (dashed blue) and $\overline{K}$ (dotted red) in presence of measurement noise.

the low-pass filter dynamics $\alpha$. Indeed, when $K^\star$ is used, the estimation fully relies on the position measure $g(\boldsymbol{d})$. This case study highlights the robustness of the TBOD compared to the LMI method. The convergence is slower with $\overline{K}$, but the precision reached is better.
*Monte Carlo simulations:* In order to extensively validate the results, a batch of 50 Monte Carlo simulations has been run with $K^\star$, $\overline{K}$, and a standard EKF. Specifically, the EKF has been implemented on $\mathcal{P}$ equations (1a), and considering $\boldsymbol{y}$ measurements in (1b) as output mapping. Thus, the EKF directly exploits the ranging measurements $\boldsymbol{d}$.
The random seeds used in these simulations differ from those used for the TBOD optimization. For the rest, the setup is the same considered in V-A. This analysis aims to validate the proposed methods' performance against the widely used EKF algorithm. As reported in Section I, we are particularly interested in reaching a good precision on the $z$ axis without compromising the estimation on $x, y$. Results are reported in Table I in terms of the average standard deviation of the estimation error, considered after convergence, namely from $\bar{t} = 30$ s. Table II reports instead the computational time required for a single iteration of each method.
Considering the EKF as the reference method, we can see that its performance on $x, y$ is not matched by the two other methods. However, the EKF performs poorly on $z$. This happens because the linearization of (1a) and (1b) depends on the distance of the material point on each axis with respect to the anchors; indeed, this value is higher on $x, y$, because of the anchor positions described in V-A. Instead, the TBOD and LMI outperform the EKF in the $z$ axis estimation. In numbers, EKF performs 52% and 75% better than TBOD

| method | $x$ axis | $y$ axis | $z$ axis | $\|\|\sigma_x, \sigma_y, \sigma_z\|\|$ |
|---|---|---|---|---|
| EKF | 0.041 m | 0.045 m | 0.188 m | 0.198 m |
| LMI $K^\star$ | 0.169 m | 0.172 m | 0.068 m | 0.250 m |
| TBOD $\overline{K}$ | 0.087 m | 0.088 m | 0.035 m | 0.129 m |

TABLE I: Performance comparison of EKF, TBOD, and LMI methods in the presence of noise. The results are from a batch of 50 Monte Carlo simulations. The first three columns report the standard deviation of the estimation error on each axis, while the fourth shows the norm.

| method | time |
|---|---|
| EKF | 0.277 s |
| LMI | 5.58e-5 s |
| TBOD | 5.6e-5 s |

TABLE II: Performance comparison of EKF, TBOD, and LMI methods in terms of computational cost. The table reports the computational time for a single iteration, expressed in seconds.

and LMI on $x$, respectively, and 48% and 73% better on $y$. Instead, EKF performs 81% and 63% worse than TBOD and LMI on $z$, respectively. Indeed, the performance improvement on $z$ is substantial for LMI and TBOD. However, TBOD outperforms LMI on all the axes, keeping a decent precision on $x, y$ as well. Overall, the estimation precision of the TBOD performs better than the EKF by 35%, as reported in the last column of Table I. Lastly, as introduced in Section II, the computational cost of TBOD and LMI methods is consistently lower than the EKF, as described in Table II. Considering all these analyses, the observer designed with TBOD is the best choice in terms of accuracy and computational cost.

## VI. Conclusions

This work proposes a hybrid observer to tackle the localization problem for a rover moving in a 3D indoor environment by using IMU measurements and ranging distances from *anchors* placed at known fixed positions. The structure of the observer relies on a static-gain $K$ whose design is critical for the estimation performance. The stability analysis of the estimation error is presented in Section III, where Theorem 1 ensures boundedness on the estimation error trajectories. As far as the design of the static-gain $K$, Section IV proposes two approaches: the LMI-based method, which we rephrased from [19] to suit our localization task, and the TBOD approach.

The theoretical part presented in Section IV is supported by the numerical results provided in Section V, comparing the precision and robustness of the two methods with a standard EKF. In particular, the TBOD approach ensures better performance, making it a valid alternative to standard tools.

Furthermore, the TBDO method can also consider nonlinearities in the plant or the observer structure, which will be explored in forthcoming research. Additionally, implementing this solution in an experimental configuration is the target of future work.

## References


[1] P. K. Panigrahi and S. K. Bisoy, "Localization strategies for autonomous mobile robots: A review," *Journal of King Saud University - Computer and Information Sciences*, vol. 34, no. 8, Part B, pp. 6019–6039, 2022.

[2] J. Aulinas, Y. Petillot, J. Salvi, and X. Lladó, "The SLAM problem: a survey," in *Artificial Intelligence Research and Development*, vol. 184, pp. 363 – 371, IOS Press Ebooks, 2008.

[3] O. Esan, S. Du, and B. Lodewyk, "Review on autonomous indoor wheel mobile robot navigation systems," in *2020 International Conference on Artificial Intelligence, Big Data, Computing and Data Communication Systems*, pp. 1–6, 2020.

[4] A. Macario Barros, M. Michel, Y. Moline, G. Corre, and F. Carrel, "A comprehensive survey of Visual SLAM algorithms," *Robotics*, vol. 11, no. 1, 2022.

[5] D. J. Yeong, G. Velasco-Hernandez, J. Barry, and J. Walsh, "Sensor and sensor fusion technology in autonomous vehicles: A review," *Sensors*, vol. 21, no. 6, 2021.

[6] L. Bianchi, D. Carnevale, R. Masocco, S. Mattogno, F. Oliva, F. Romanelli, and A. Tenaglia, "Efficient visual sensor fusion for autonomous agents," in *2023 International Conference on Control, Automation and Diagnosis (ICCAD)*, 2023.

[7] F. Dieter, W. Burgard, and S. Thrun, "Markov localization for mobile robots in dynamic environments," *Journal of Artificial Inteligence Research*, vol. 11, pp. 391–427, 1999.

[8] E. Menegatti, A. Zanella, S. Zilli, F. Zorzi, and E. Pagello, "Range-only SLAM with a mobile robot and a wireless sensor networks," in *IEEE Int. Conf. Robot. Autom.*, pp. 8–14, May 2009.

[9] J. J. L. E. Olson and S. Teller, "Robust range-only beacon localization," *IEEE Journal of Oceanic Engineering*, 2006.

[10] M. J. Segura, F. A. Auat Cheein, J. M. Toibero, V. Mut, and R. Carelli, "Ultra Wide-Band localization and SLAM: A comparative study for mobile robot navigation," *Sensors*, vol. 11, no. 2, pp. 2035–2055, 2011.

[11] Q. Shi, X. Cui, W. Li, Y. Xia, and M. Lu, "Visual-UWB navigation system for unknown environments," *ION GNSS+, The International Technical Meeting of the Satellite Division of The Institute of Navigation*, Oct 2018.

[12] A. Kaczmarek, W. Rohm, L. Klingbeil, and J. Tchórzewski, "Experimental 2D extended Kalman Filter sensor fusion for low-cost GNSS/IMU/Odometers precise positioning system," *Measurement*, vol. 193, p. 110963, 2022.

[13] K. T and P. TH, "Extended Kalman Filter (EKF) design for vehicle position tracking using reliability function of radar and lidar," *Sensors (Basel)*, 2020.

[14] L. Armesto, S. Chroust, M. Vincze, and J. Tornero, "Multi-rate fusion with vision and inertial sensors," in *IEEE International Conference on Robotics and Automation, 2004. Proceedings. ICRA '04. 2004*, vol. 1, pp. 193–199 Vol.1, 2004.

[15] L. Armesto, J. Tornero, and M. Vincze, "On multi-rate fusion for non-linear sampled-data systems: Application to a 6D tracking system," *Robotics and Autonomous Systems*, vol. 56, no. 8, pp. 706–715, 2008.

[16] A. I. Mourikis and S. I. Roumeliotis, "A multi-state constraint Kalman Filter for vision-aided inertial navigation," in *Proceedings 2007 IEEE international conference on robotics and automation*, pp. 3565–3572, IEEE, 2007.

[17] A. Barrau and S. Bonnabel, "The invariant Extended Kalman Filter as a stable observer," *IEEE Transactions on Automatic Control*, vol. 62, no. 4, p. 1797 – 1812, 2017.

[18] R. Goebel, R. G. Sanfelice, and A. R. Teel, "Hybrid dynamical systems," *IEEE control systems magazine*, vol. 29, no. 2, pp. 28–93, 2009.

[19] A. Sferlazza, S. Tarbouriech, and L. Zaccarian, "Time-varying sampled-data observer with asynchronous measurements," *IEEE Transactions on Automatic Control*, vol. 64, no. 2, pp. 869–876, 2018.

[20] F. Alonge, F. D'Ippolito, G. Garraffa, and A. Sferlazza, "A hybrid observer for localization of mobile vehicles with asynchronous measurements," *Asian Journal of Control*, vol. 21, no. 4, pp. 1506–1521, 2019.

[21] S. Berkane and A. Tayebi, "Attitude estimation with intermittent measurements," *Automatica*, vol. 105, pp. 415–421, 2019.

[22] M. Wang and A. Tayebi, "Nonlinear state estimation for inertial navigation systems with intermittent measurements," *Automatica*, vol. 122, p. 109244, 2020.

[23] Y. Zhou, "An efficient least-squares trilateration algorithm for mobile robot localization," in *2009 IEEE/RSJ International Conference on Intelligent Robots and Systems*, pp. 3474–3479, IEEE, 2009.